

ARCHETYPAL ANALYSIS FOR SPARSE REPRESENTATION-BASED HYPERSPECTRAL SUB-PIXEL QUANTIFICATION

Lukas Drees^{a,*}; Ribana Roscher^a

^a Institute of Geodesy and Geoinformation, Remote Sensing Group, University of Bonn, Germany - (s7ludree, ribana.roscher)@uni-bonn.de

KEY WORDS: Archetypal analysis, sparse representation, sub-pixel quantification

ABSTRACT:

This paper focuses on the quantification of land cover fractions in an urban area of Berlin, Germany, using simulated hyperspectral EnMAP data with a spatial resolution of 30m×30m. For this, sparse representation is applied, where each pixel with unknown surface characteristics is expressed by a weighted linear combination of elementary spectra with known land cover class. The elementary spectra are determined from image reference data using simplex volume maximization, which is a fast heuristic technique for archetypal analysis. In the experiments, the estimation of class fractions based on the archetypal spectral library is compared to the estimation obtained by a manually designed spectral library by means of reconstruction error, mean absolute error of the fraction estimates, sum of fractions and the number of used elementary spectra. We will show, that a collection of archetypes can be an adequate and efficient alternative to the spectral library with respect to mentioned criteria.

INTRODUCTION

The estimation of the degree of imperviousness as an indicator of environmental quality is subject of current research towards a time and cost efficient monitoring of urban areas (Weng, 2012). Remote sensing data, such as imaging spectroscopy, builds a valuable basis to comprehensively map urban areas and quantify the imperviousness based on the spectral information (e.g., Huang et al. (2014); Roessner et al. (2011)). Especially, hyperspectral imagery is a well suited source for mapping of such areas, because it offers a high spectral separability of different materials. However, generally, the temporal and spatial resolution is limited in comparison to sensors with lower spectral resolution. These limitations are partially overcome with the launch of missions such as Environmental Mapping and Analysis Program (EnMAP), which increases the availability of hyperspectral data and therefore the temporal resolution (Guanter et al., 2015). Nevertheless, due to its spatial resolution, the provided data is mainly characterized by spectrally mixed pixels, which demands sophisticated sub-pixel quantification approaches in order to estimate the fraction of various land cover classes in each pixel.

In this context, several approaches have been developed comprising regression approaches (Okujeni et al., 2016b; Priem et al., 2016), probabilistic classification methods (Rosentreter et al., 2017; Suess et al., 2014), and the usage of spectral libraries for spectral mixture analysis (Somers et al., 2011; Powell et al., 2007). An overview of a wide variety of unmixing approaches can be found in e.g. Bioucas-Dias et al. (2012). While the latter approach needs a spectral library containing elementary spectra of known materials, the first two approaches also require mixed spectra for learning an appropriate model. These mixed spectra can be derived from the image using information about known mixed pixels, or from synthetically mixed pixel, as been presented in Rosentreter et al. (2017) and Okujeni et al. (2016b).

A critical step is the extraction of the elementary spectra. A manual extraction is time-consuming and requires human expert-knowledge and therefore, automatic extraction techniques have

been an active field of research during the past decade (e.g., Bioucas-Dias et al. (2012); Veganzones and Grana (2008)). Most of the algorithms rely on the assumption that the elementary spectra lie on a convex hull or a convex polytope enclosing the data distribution (e.g., Chan et al. (2011); Craig (1994)). Based on this assumption all data samples can be reconstructed by a non-negative linear combination of the elementary spectra. A promising approach from this group used for unmixing is so-called archetypal analysis, which searches for extreme points in the data distribution (Zhao et al., 2017, 2016). Besides the actual determination of elementary spectra, other challenges exist which need to be tackled: The number of elementary spectra is unknown beforehand and thus, a suitable amount of spectra needs to be extracted to make the set representative enough, but also small enough to keep the sub-pixel quantification robust and efficient. Moreover, many extraction techniques depend on the initialization and thus, a strategy needs to be defined to ensure a stable result (e.g., Wang et al. (2016); Zortea and Plaza (2009)).

In this paper, a sub-pixel quantification of an urban area is performed, aiming at the estimation of a fraction map containing the classes *impervious surface*, *vegetation*, *soil* and *water*. The set of elementary spectra is obtained by archetypal analysis (Mørup and Hansen, 2012; Cutler and Breiman, 1994), where a simplex volume maximization (SiVM) heuristic is used (Thureau et al., 2010). Archetypal analysis fulfills the above mentioned requirements, such that it is able to find an appropriate number of elementary spectra and initialization techniques can be found to be robust against different initial values. In our experiments, the sub-pixel quantification is obtained by applying sparse representation using elementary spectra derived from (1) a manually designed spectral library, and (2) an automatically determined set of archetypes. As study site, a freely available simulated EnMAP scene is used, which was acquired over the city of Berlin, Germany (Okujeni et al., 2016a)¹. The simulated EnMAP scene has a spectral resolution from 0.45 μ m to 2.5 μ m, and a spatial resolution of 30m×30m. Both spectral libraries are derived from the given image data only in order to show the comparability of data-

¹<http://pmd.gfz-potsdam.de/enmap/showshort.php?id=escidoc:1480925>

*Corresponding author

adapted libraries. We will show that the automatically extracted elementary spectra yield similar or better results in comparison to the manually designed spectral library, and thus states a fast alternative for sub-pixel quantification.

METHODS

The following section describes the sub-pixel quantification of an urban area using sparse representation and archetypal analysis. Archetypal analysis is used to determine the extreme points of the data distribution, which are used within the sparse representation approach to estimate the fractions of land cover classes in each pixel.

Archetypal Analysis with Simplex Volume Maximization

The extraction of the archetypes $A = [\mathbf{a}_1, \dots, \mathbf{a}_k, \dots, \mathbf{a}_K]$, $k = 1, \dots, K$, is carried out by simplex volume maximization (SiVM), which is an efficient method to determine the extreme points (so-called archetypes) of the data distribution. This approach is aiming on an approximation of the convex hull, where all archetypes are located on it. We have given a $(M \times N)$ -dimensional data matrix X , in which N is the number of reference pixels $X = [\mathbf{x}_1, \dots, \mathbf{x}_N]$ with given land cover class c_n , and M is the pixel dimension. In order to find the first archetype, the approach is initialized with the mean vector \mathbf{a}_0 of all data samples X . The pixel with maximal distance to \mathbf{a}_0 , is defined as first archetype (Step 1).

$$\mathbf{a}_1 = \arg \max_n d(\mathbf{a}_0, \mathbf{x}_n), \quad (1)$$

with $d(\cdot, \cdot)$ being the Euclidean distance function between the spectral features of the archetype \mathbf{a}_0 and the pixel \mathbf{x}_n . Other distance functions are possible, e.g. to account for different intra-class variabilities of various spectra. Further archetypes are specified sequentially, such that the volume of the simplex becomes maximized with each additional archetype. Since this volume operation is too computational intense, the archetypes are selected to have maximum distance to all previously detected ones.

$$\mathbf{a}_M = \arg \max_n d(A, \mathbf{x}_n) \quad (2)$$

The number of archetypes is generally not known beforehand, and depends on the number of informative dimensions and the variability of the data. In order to find a suitable set of archetypes, the dataset is outlier-cleaned using the local outlier factor approach (Breunig et al., 2000).

Sparse Representation

In order to determine the sub-pixel fractions, we use sparse representation with non-negative least squares optimization. In terms of sparse coding a sample \mathbf{x}_s , $s = 1, \dots, S$, is represented by a weighted linear combination of a few elements taken from a $(M \times T)$ -dimensional dictionary D , such that $\mathbf{x}_s = D\boldsymbol{\alpha}_s + \boldsymbol{\gamma}$ with $\|\boldsymbol{\gamma}\|_2$ being the reconstruction error. The dictionary $D = [\mathbf{x}_1, \dots, \mathbf{x}_t, \dots, \mathbf{x}_T]$ is embodied by the archetypes. The coefficient vector, comprising the activations, is given by $\boldsymbol{\alpha}_s$. The activations are interpreted as class fractions for sub-pixel quantification. The optimization problem for the determination of optimal $\hat{\boldsymbol{\alpha}}_s$ is given by

$$\hat{\boldsymbol{\alpha}}_s = \arg \min \|D\boldsymbol{\alpha}_s - \mathbf{x}_s\|_2, \quad (3)$$

$$\text{subject to } \boldsymbol{\alpha}_s \succeq \mathbf{0}, \sum_s \boldsymbol{\alpha}_s = 1, \quad (4)$$

where the first term is the reconstruction error and the second and third term are the non-negativity constraint and the sum-to-1 constraint. Generally, (3) leads to dense solutions and sparsity-enforcing priors such as an L_1 -norm or L_0 -norm of the parameters are introduced. However, since non-negativity alone leads to a sufficient sparsity, we do not introduce a further sparsity enforcing prior.

EXPERIMENTS

Data

Our studies are performed using the Berlin-Urban-Gradient dataset Okujeni et al. (2016a), illustrated in Fig. 1. The dataset consists of a hyperspectral image, a simulated EnMAP scene, a manually derived spectral library, reference land cover information and reference fractions for evaluation.

3.1.1 HyMap Data The hyperspectral image was acquired from the Hyperspectral Mapper (HyMap), and serve as basis for the extracting of the archetypes. The study site is the Southwest of Berlin, Germany, with a spatial resolution of 3.6m. The HyMap image consists of 126 spectral bands, however, 15 noisy bands were removed resulting in 111 bands used for this work. The observed wavelengths are ranging from $0.45\mu\text{m}$ to $2.5\mu\text{m}$, showing a high spectral information diversity, which enables a detailed analysis of the urban structure. In addition to the HyMap image, a manually derived reference image containing 112.690 reference pixel is provided with valuable spectra, each labeled with one of the four land cover classes: **impervious surface**, **vegetation**, **soil** and **water**. The reference information is manually obtained by using digital orthophotos and cadastral data.

3.1.2 Simulated EnMAP Data EnMAP is German hyperspectral satellite mission, which will start not earlier than 2018, with a focus on earth environmental observations in a global scale. Based on the HyMap data, an EnMAP scene was simulated using EnMAP End-to-End Simulation tool (EeteS, Segl et al. (2012)). The spatial resolution of 30m is lower than the resolution of the HyMap scene, and thus the mixing of land cover classes are more apparent. Just as the HyMap data EnMAP has a spectral resolution from $0.45\mu\text{m}$ to $2.5\mu\text{m}$. For evaluation purposes, 1495 EnMAP pixels were obtained from the the simulation tool, containing the fractions of the land cover classes ranging from 0 to 100%.

3.1.3 Manually Designed Spectral Library The spectral library is a manually designed collection of 75 pure spectra obtained from the HyMap image. The spectra contain different land cover classes with 39 impervious surface spectra (different types of roof, pavement, tartan, pool water), 31 vegetation spectra (grass, tree), 4 soil spectra (uncovered ground, sand) and one natural water spectrum. All together, it is a balanced library for urban structures with 39 impervious and 36 pervious spectra. All spectra in the library can be assigned to a hierarchical urban classification scheme, which was developed by Heiden et al. (2007). First, an initial collection of 300 spectra was selected by expert knowledge. Afterwards a two-step filtering was performed, in which the variability between the spectra is maximized in consideration of spectral variability of materials, brightness and shading

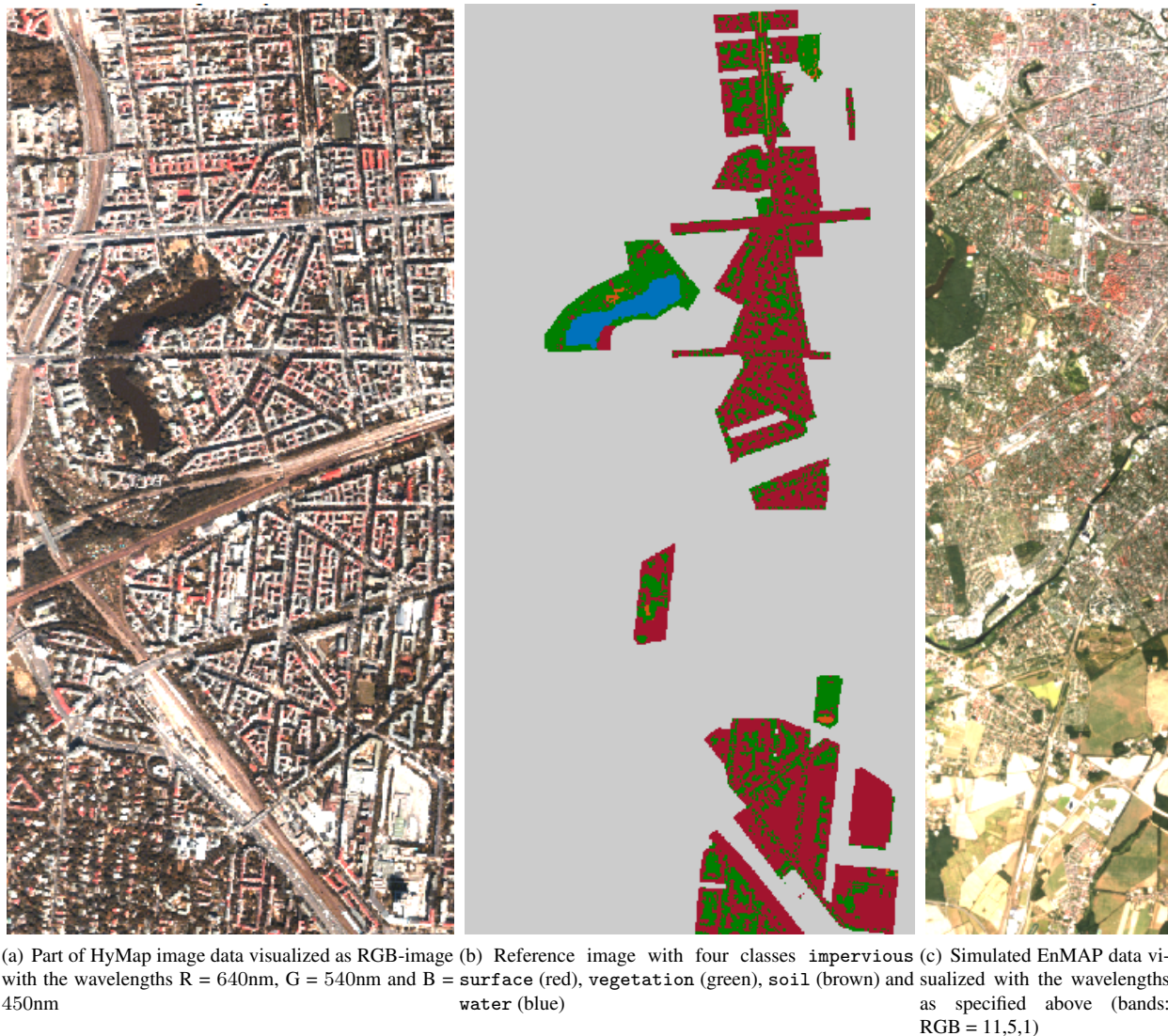


Figure 1. Berlin-Urban-Gradient dataset

effects. Moreover, in an iterative process those spectra for the final subset were selected that best describes the spectral diversity in a specific neighborhood. More details can be found in Okujeni et al. (2016a).

Experimental Setup

In our experiments the simulated EnMAP data is reconstructed by sparse representation using (1) the manually designed spectral library and (2) the automatically derived set of archetypes. The aim of the experiments is to show the suitability of the spectral libraries for sub-pixel quantification. Moreover, the goal is to show that the set of archetypes achieves a similar good or a better result than the manually designed spectral library. The sub-pixel quantification is evaluated with the given reference mixing fractions. Additionally, the number of used archetypes is evaluated and discussed. For this, two different sets of archetypes are used. The first set \mathcal{A}_1 , contains all archetypes, extracted as presented in the previous section. The second set \mathcal{A}_2 , contains 50% of all archetypes in \mathcal{A}_1 , comprising only the archetypes with the smallest distance to the class-specific mean. Using the second set, we simulate datasets, which do not have a great variability in the feature space resulting in less archetypes. In summary,

three different dictionaries, namely AA-R (using \mathcal{A}_1 and \mathcal{A}_2) and the manually designed spectral library Lib are used for sub-pixel quantification with sparse representation. In order to guarantee an extraction of valuable archetypes, which are no outliers, the local outlier factor is applied, using 10 neighbors and a quantile of 0.8 as threshold on the pairwise distances.

Evaluation

For evaluation, several statistics are provided. First, the reconstruction error of the sparse representation is provided, indicating the ability of the elementary spectra to represent the EnMAP pixels. Moreover, the result of the sparse representation is evaluated by a comparison between reference and actual estimated fraction coefficients. In this way, a measure is provided to evaluate the assignments to the correct land cover class. This is done by means of the overall and class-wise mean absolute error (MAE) between reference and actual coefficients.

$$\text{MAE} = \frac{1}{S} \sum_{i=1}^S |(\alpha_i - \alpha_s)|, \quad (5)$$

with α_i being the reference fractions, α_s being the estimated fractions, and S being the number of evaluated pixels. The

Table 1. Overall (\varnothing) and class-wise MAE, reconstruction error $\|\gamma\|_2$, and class-wise sum over all fractions based on the sub-pixel quantification of the EnMAP reference data. In the first two rows are the results for the archetypal reconstruction using a different number of archetypes (40 and 20) contained in the set \mathcal{A}_1 and the set \mathcal{A}_2 , denoted by AA-R. The last row contains the results for the reconstruction using the manually designed spectral library (Lib) with all contained spectra (75). Bold numbers indicate the best results.

	Amount	$\ \gamma\ _2$	class-wise MAE [%]				\varnothing MAE [%]	coefficient sum over all pixel			
			imp. surface	vegetation	soil	water		imp. surface	vegetation	soil	water
AA-R	40	1,1	12,2	11,0	2,5	1,9	6,8	766,2	669,2	21,3	36,8
AA-R	20	1,2	13,6	10,8	1,8	6,1	8,1	658,1	704,9	17,8	112,2
Lib	75	0,0	16,0	9,2	2,1	12,2	9,9	556,9	695,4	32,0	208,8
True values of EnMAP data								754,8	674,4	27,0	36,8

smaller the MAE, the better the reconstruction by sparse representation. Moreover, the class-wise sum of the class fractions is provided.

Results and Discussion

3.4.1 Archetypal Analysis

The total number and the quality of the archetypes have a significant influence on the success of the sparse representation. In theory, it is generally not known beforehand how many archetypes can be generated from the data. It depends primarily on the data dimension and the inner variability of the data distribution. In our experiments, the archetypes are extracted from the given reference image (see Sec. 3.1.1), which is previously outlier-cleaned as specified in Sec. 3.2.

Given the data, the number of extracted archetypes in set \mathcal{A}_1 is 40 and the number in set \mathcal{A}_2 is 20, which both serve as elementary spectra included in the dictionary D . The first archetype set \mathcal{A}_1 consists of 25 impervious surface spectra, 12 vegetation spectra, 2 soil spectra and one water spectrum. Except the water spectrum, the amount is class-wise halved (12 impervious surface spectra, 6 vegetation spectra, 1 soil spectra, 1 water spectrum) to create the second set \mathcal{A}_2 . We observed that an extraction of more than 40 archetypes means that some archetypes lie in the center of the dataset X . The reason for this is that from a certain point on, positions in the center of X have the maximal distance to the previously extracted archetypes.

3.4.2 Sub-pixel Quantification

Table 1 presents the results of the EnMAP sub-pixel quantification. The MAE shows that all three dictionaries achieve a similar and satisfactory solution. The archetypes have a smaller class-wise MAE for **impervious surface** and **water**, whereas the spectral library has a better result for **vegetation**. **Soil** is reconstructed with a low MAE by all approaches. However, the average MAE obtained from both archetypal sets is better (7% and 8%) than from the spectral library (10%), even though there are more elementary spectra used for sub-pixel quantification. We assume that some entries in the spectral library are less helpful, because they are either not representative enough, or they do not fit to the observed pixel, or they do not contain additional information with respect to the other spectra. However, the high number of elementary spectra results in a small reconstruction error. On the right side of Table 1 we provide the coefficient sum over all pixel. Compared to the true values of EnMAP data, the reconstruction using set \mathcal{A}_1 leads to the smallest differences in the classes **imp. surface**, **vegetation** and **water**. With respect to our goal to quantify the sub-pixel fractions there is no direct relation to the MAE. It is possible to obtain a correct coefficient sum and a MAE, even if

the amount of under- and overestimated fractions is large, exactly when the fractions are in equal share.

Figure 2 shows the class-wise fraction estimates, opposed to the reference fractions. There are 1495 dots in each plot. It can be observed that **soil** and **water** have a high proportion of 0% reference fractions and lesser $>0\%$ fractions than **impervious surface** and **vegetation**. The **impervious surface** scatter plot show that for AA-R-40 the two lines intersect nearly the 55% point on the x-axis. This means that the estimated fractions are usually too high for all pixels which have a degree of impervious surfaces over 55%, and otherwise too small for smaller values than the intersection point. In comparison to AA-R-20 and Lib, where the reference values are mostly underestimated, the first set of archetypes \mathcal{A}_1 shows the best result for **impervious surface**. The **vegetation** scatter plots do not have large discrepancies between the true 1:1 line (dashed line) and the estimated least-squares regression line (solid line), and the obtained results are similar for all used sets of elementary spectra. Additionally, the scatter plots for **soil** look similar, but overall not as good as for the other three classes. As specified above there is a high amount of 0% fractions, which are estimated with up to 30% when using the AA-R-40 spectra and Lib and 40% fractions when using AA-R-20 spectra. Furthermore, all pixels with **soil**-fractions are clearly underestimated equally. We assume that the small number of elementary spectra is insufficient for the spectral diversity of **soil** pixels. Finally, the described observation with high estimated 0% fractions also occurs in the **water** class with values over 90% (AA-R-20). This is more apparent for Lib and AA-R-20 than for AA-R-40. However, the underestimation of the remaining pixels is smaller in Lib than in AA-R-40 and AA-R-20.

Figure 4 shows the degree of imperviousness in an exemplarily part of the EnMAP scene. The fraction map of the **impervious surface** is visualized as gray value image. It is apparent that the left fraction map, derived by AA-R-40, is much brighter than this one obtained by Lib. Thus, the degree of imperviousness of 50.6% for AA-R-40 is higher than 35.1% for Lib. Despite the fact that the actual degree of imperviousness is not given for this part from Berlin, the sum of all fractions is given for the reference pixels in Table 1 and can be used for comparison. The reference value of 754,8 for **impervious surface** is slightly overestimated by AA-R-40, but clearly underestimated by 200 by Lib.

Figure 3 illustrates how often each spectrum is used for reconstruction for the determination of the fractions in 1493 EnMAP pixels. AA-R-40 shows that there are significant elementary spectra, e.g., 10, 29 and 31, which often have a high fraction in the

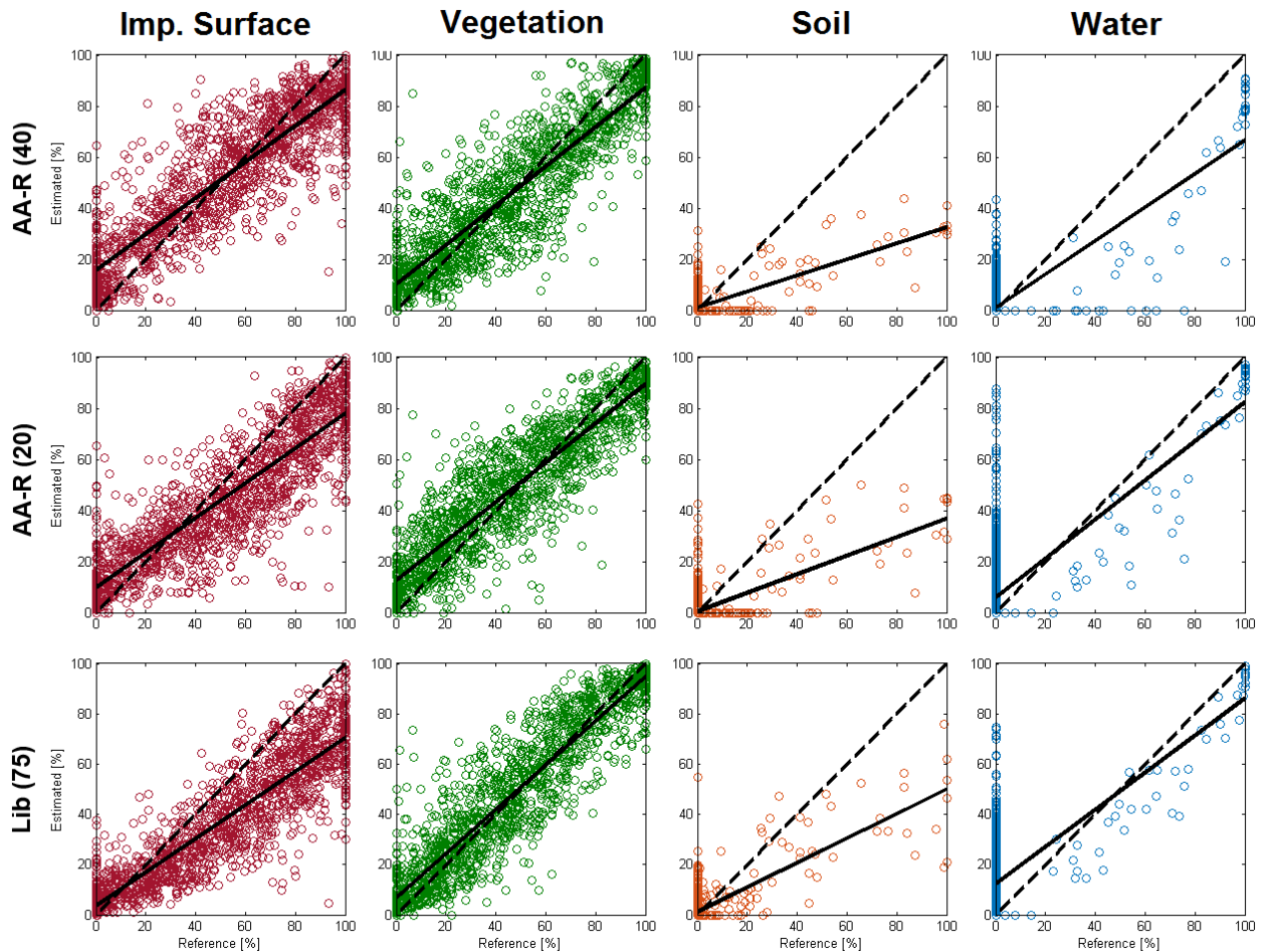


Figure 2. Scatter plots representing the class-wise fraction estimates of **impervious surface**, **vegetation**, **soil** and **water**, opposed to the reference fractions. A correct estimated pixel lies on the dashed line. The solid line represents the respective least-square regression line for the scatter points.

reconstruction. In the other side, there are some elementary spectra in all plots which are used rarely. It can be observed that there is generally no dependence between the height of a bar, i.e. the number of non-zero estimated fractions for the spectra, and its overall fraction's sum for all pixels. A striking example is spectra 3 in the AA-R-40 plot. It is used for more than 1200 pixel reconstructions, but its fraction's sum is only one third in comparison to spectra 10, which shows a similar high amount of uses. Especially noticeable are the differences in the bar for the class **water** between the manually designed library and the archetypes. A water spectrum has the special characteristic that there are only small reflectance values over all bands, so that it acts almost as a linear factor. Because of this, it is well suited to support all reconstructions, resulting in a high overall fraction sum. Its value in the manually designed spectral library is high with a fraction's sum over 200, in comparison to AA-R-40 which shows a sum of fractions identical to the true value (see Table 1). For AA-R-20 the sum of water fractions is higher than for AA-R-40. We assume the reason for this is the less number of elementary spectra, where oftentimes a reconstruction with water spectra is helpful regardless of the presence of water in the pixel.

We can also compare our results to Rosentreter et al. (2017), who use more sophisticated classification and regression techniques to reconstruct the EnMAP data with the same spectral library Lib. When using Import or Support Vector Machines the overall MAE

(8,65% and 10,22%) is slightly worse than AA-R. Similar results yield the regression techniques Support Vector Regression (10,06%) and Multioutput Support Vector Regression (6,92%). The computing time is many hours in contrast to a few minutes in this work. Considering the computational cost of those approaches the quality of our results is remarkable.

CONCLUSION

This paper presented a sub-pixel quantification of the urban area of Berlin, Germany, into the four land cover classes **impervious surface**, **vegetation**, **soil** and **water**. The quantification was performed by sparse representation using elementary spectra derived from (1) a manually designed spectral library, and (2) an automatically determined set of archetypes. The archetypes were extracted from HyMap data with given reference information for all land cover classes. For this, simplex volume maximization was used, a fast approximation to archetypal analysis. In our experiments, we could show that the extracted archetypes are suitable to serve as spectral library for sparse representation. In contrast to a manually derived library they have the advantage that they can be easily extracted, and they are adapted to the current image characteristics, in case reference data is given. The results demonstrate in average a less mean absolute error for the archetypal sets \mathcal{A}_1 (6.8%) and \mathcal{A}_2 (8.1%), in comparison to the manually designed library Lib (9.9%), although the latter one contains

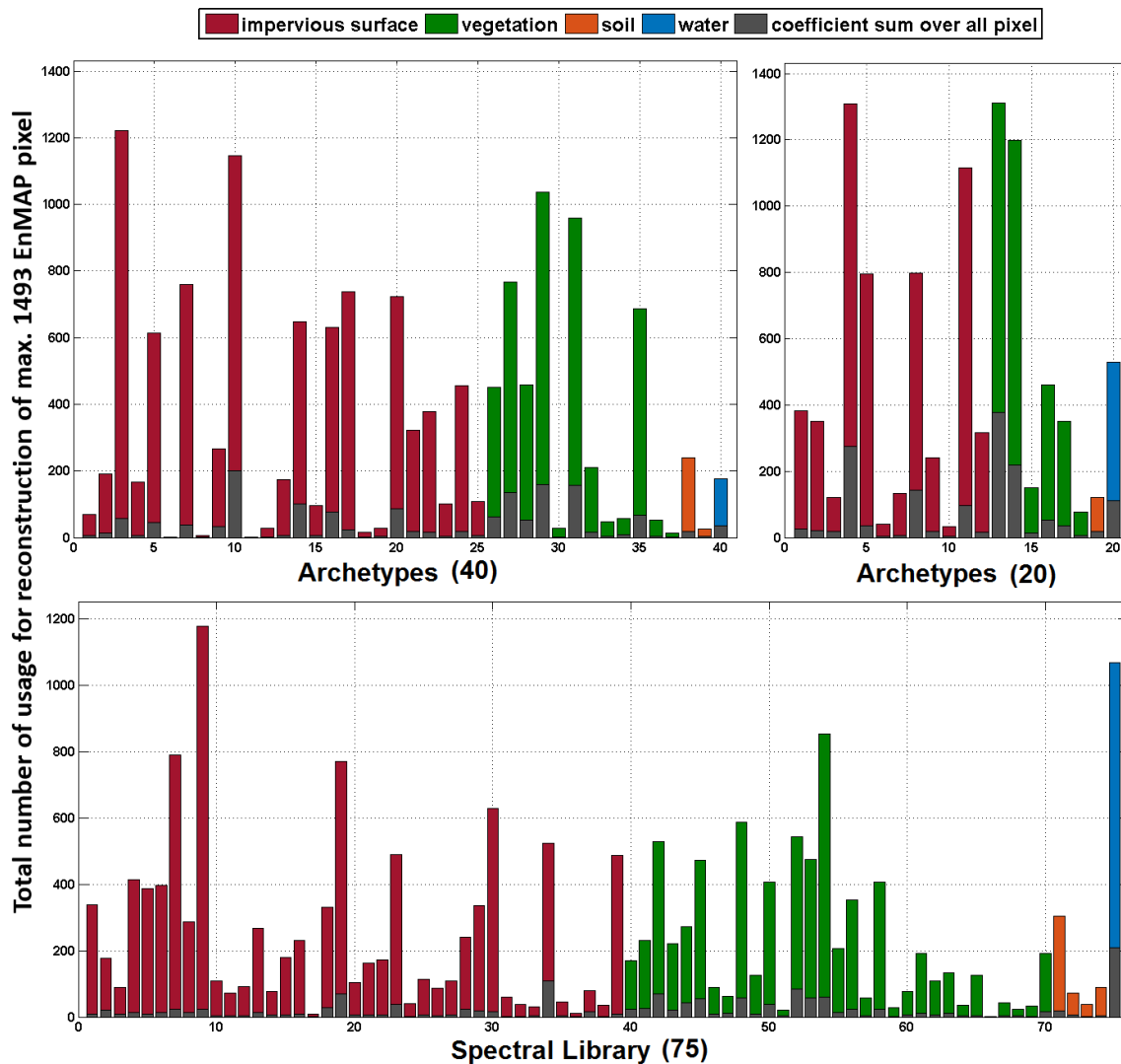


Figure 3. The figure shows how often a elementary spectra is used for reconstruction of the reference EnMAP pixels. The maximal possible height of a bar is 1493, if the elementary spectrum would be involved in the reconstruction of all reference EnMAP pixels. The grew parts specify the sum of the fractions (i.e., the estimated coefficients) over all pixel.

more elementary spectra. Moreover the class-wise results shows mostly a good estimation of class fractions for *imp. surface* and *vegetation*, but an underestimation for *soil* and *water* for all used libraries.

In summary, the automatically extracted archetypal spectral library is an adequate alternative to a manually derived spectral library. In case no reference data is given, the interpretation can be done in a fast way by assigning land cover classes to the extracted archetypes using expert knowledge. The presented approach can also be combined with spatial information, which may further increase the approximation ability and accuracy of the fraction estimates. A worthwhile direction of further investigations is the combination of archetypal analysis with more sophisticated models for sub-pixel quantification.

ACKNOWLEDGEMENTS

The authors would like to thank Akpona Okujeni, Sebastian van der Linden and Patrick Hostert for providing the dataset. Moreover, the authors would like to thank Johannes Rosentreter for valuable discussions.

References

- Bioucas-Dias, J. M., Plaza, A., Dobigeon, N., Parente, M., Du, Q., Gader, P. and Chanussot, J., 2012. Hyperspectral unmixing overview: Geometrical, statistical, and sparse regression-based approaches. *IEEE Journal of Selected Topics in Applied Earth Observations and Remote Sensing* 5(2), pp. 354–379.
- Breunig, M. M., Kriegel, H.-P., Ng, R. T. and Sander, J., 2000. Lof: Identifying density-based local outliers. *SIGMOD Rec.* 29(2), pp. 93–104.
- Chan, T.-H., Ma, W.-K., Ambikapathi, A. and Chi, C.-Y., 2011. A simplex volume maximization framework for hyperspectral endmember extraction. *IEEE Transactions on Geoscience and Remote Sensing* 49(11), pp. 4177–4193.
- Craig, M. D., 1994. Minimum-volume transforms for remotely sensed data. *IEEE Transactions on Geoscience and Remote Sensing* 32(3), pp. 542–552.
- Cutler, A. and Breiman, L., 1994. Archetypal analysis. *Technometrics* 36(4), pp. 338–347.
- Guanter, L., Kaufmann, H., Segl, K., Foerster, S., Rogass, C., Chabrillat, S., Kuester, T., Hollstein, A., Rossner, G., Chlebek,

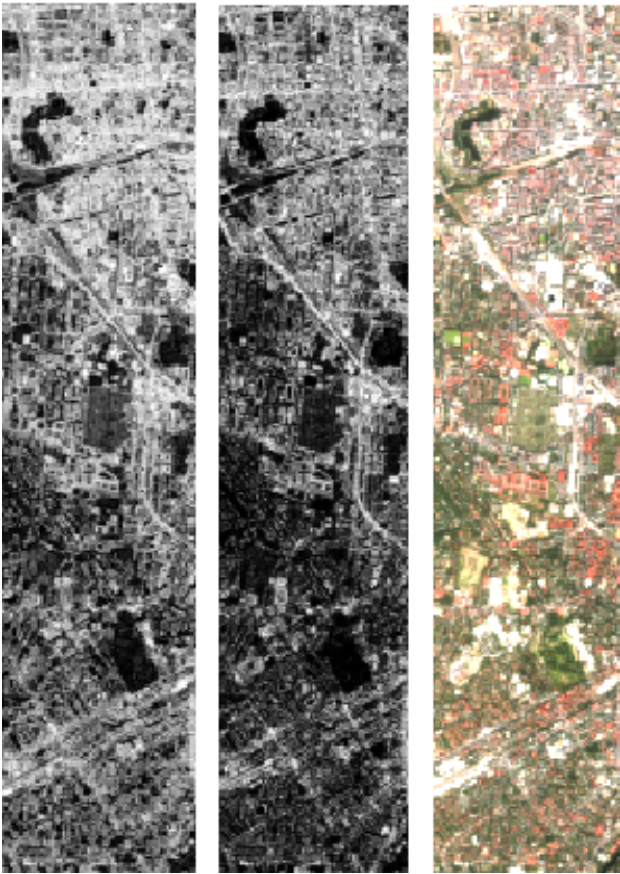


Figure 4. Fraction maps of impervious surface in an exemplarily part of the EnMAP scene to estimate the degree of imperviousness derived by AA-R-40 (left) and Lib (middle). The pixel-wise degree of imperviousness lies between 0% (black) and 100% (white). The right image shows the corresponding EnMAP-scene is plotted (RGB = 11,5,1).

- C. et al., 2015. The enmap spaceborne imaging spectroscopy mission for earth observation. *Remote Sensing* 7(7), pp. 8830–8857.
- Heiden, U., Segl, K., Roessner, S. and Kaufmann, H., 2007. Determination of robust spectral features for identification of urban surface materials in hyperspectral remote sensing data. *Remote Sensing of Environment* 111(4), pp. 537–552.
- Huang, X., Lu, Q. and Zhang, L., 2014. A multi-index learning approach for classification of high-resolution remotely sensed images over urban areas. *ISPRS Journal of Photogrammetry and Remote Sensing* 90, pp. 36–48.
- Mørup, M. and Hansen, L. K., 2012. Archetypal analysis for machine learning and data mining. *Neurocomputing* 80, pp. 54–63.
- Okujeni, A., van der Linden, S. and Hostert, P., 2016a. Berlin-urban-gradient dataset 2009 - an enmap preparatory flight campaign (datasets). GFZ Data Services.
- Okujeni, A., van der Linden, S., Suess, S. and Hostert, P., 2016b. Ensemble learning from synthetically mixed training data for quantifying urban land cover with support vector regression. *IEEE Journal of Selected Topics in Applied Earth Observations and Remote Sensing*.
- Plaza, A., Martínez, P., Pérez, R. and Plaza, J., 2004. A quantitative and comparative analysis of endmember extraction algorithms from hyperspectral data. *IEEE transactions on geoscience and remote sensing* 42(3), pp. 650–663.
- Powell, R. L., Roberts, D. A., Dennison, P. E. and Hess, L. L., 2007. Sub-pixel mapping of urban land cover using multiple endmember spectral mixture analysis: Manaus, Brazil. *Remote Sensing of Environment* 106(2), pp. 253–267.
- Priem, F., Okujeni, A., van der Linden, S. and Canters, F., 2016. Use of multispectral satellite imagery and hyperspectral endmember libraries for urban land cover mapping at the metropolitan scale. In: *SPIE Remote Sensing*, International Society for Optics and Photonics.
- Roessner, S., Segl, K., Bochow, M., Heiden, U., Heldens, W. and Kaufmann, H., 2011. Potential of hyperspectral remote sensing for analyzing the urban environment. *Urban remote sensing: Monitoring, synthesis and modeling in the urban environment* pp. 49–61.
- Rosentreter, J., Hagensieker, R., Okujeni, A., Roscher, R. and Waske, B., 2017. Sub-pixel mapping of urban areas using enmap data and multioutput support vector regression. *IEEE Journal of Selected Topics in Applied Earth Observations and Remote Sensing*. to appear.
- Segl, K., Guanter, L., Rogass, C., Kuester, T., Roessner, S., Kaufmann, H., Sang, B., Mogulsky, V. and Hofer, S., 2012. Eetes-the enmap end-to-end simulation tool. *IEEE Journal of Selected Topics in Applied Earth Observations and Remote Sensing* 5(2), pp. 522–530.
- Somers, B., Asner, G. P., Tits, L. and Coppin, P., 2011. Endmember variability in spectral mixture analysis: A review. *Remote Sensing of Environment* 115(7), pp. 1603–1616.
- Suess, S., van der Linden, S., Leitao, P. J., Okujeni, A., Waske, B. and Hostert, P., 2014. Import vector machines for quantitative analysis of hyperspectral data. *IEEE Geoscience and Remote Sensing Letters* 11(2), pp. 449–453.
- Thurau, C., Kersting, K. and Bauckhage, C., 2010. Yes we can: simplex volume maximization for descriptive web-scale matrix factorization. In: *Proceedings of the 19th ACM international conference on information and knowledge management*, ACM, pp. 1785–1788.
- Veganzones, M. A. and Grana, M., 2008. Endmember extraction methods: A short review. In: *International Conference on Knowledge-Based and Intelligent Information and Engineering Systems*, Springer, pp. 400–407.
- Wang, R., Li, H., Liao, W. and Huang, X., 2016. Endmember initialization method for hyperspectral data unmixing. *Journal of Applied Remote Sensing* 10(4), pp. 042009.
- Weng, Q., 2012. Remote sensing of impervious surfaces in the urban areas: Requirements, methods, and trends. *Remote Sensing of Environment* 117, pp. 34–49.
- Zhao, C., Zhao, G. and Jia, X., 2017. Hyperspectral image unmixing based on fast kernel archetypal analysis. *IEEE Journal of Selected Topics in Applied Earth Observations and Remote Sensing* 10(1), pp. 331–346.
- Zhao, G., Zhao, C. and Jia, X., 2016. Multilayer unmixing for hyperspectral imagery with fast kernel archetypal analysis. *IEEE Geoscience and Remote Sensing Letters* 13(10), pp. 1532–1536.
- Zortea, M. and Plaza, A., 2009. A quantitative and comparative analysis of different implementations of n-findr: A fast endmember extraction algorithm. *IEEE Geoscience and Remote Sensing Letters* 6(4), pp. 787–791.